Editors' Suggestion

Infrared Magnetopolaritons in $MoTe_2$ Monolayers and Bilayers

Bo Han,[1] Jamie M. Fitzgerald,[2] Lukas Lackner,[1] Roberto Rosati,[2] Martin Esmann,[1] Falk Eilenberger,[3,4,5] Takashi Taniguchi,[6] Kenji Watanabe,[7] Marcin Syperek,[8] Ermin Malic,[2] and Christian Schneider[1,*]

[1]*Institut für Physik, Fakultät V, Carl von Ossietzky Universität Oldenburg, 26129 Oldenburg, Germany*
[2]*Department of Physics, Philipps-Universität Marburg, Mainzer Gasse 33, D-35032 Marburg, Germany*
[3]*Fraunhofer-Institute for Applied Optics and Precision Engineering IOF, 07745 Jena, Germany*
[4]*Institute of Applied Physics, Abbe Center of Photonics, Friedrich Schiller Universität Jena, 07745 Jena, Germany*
[5]*Max Planck School of Photonics, 07745 Jena, Germany*
[6]*International Center for Materials Nanoarchitectonics, National Institute for Materials Science, Tsukuba 305-0044, Japan*
[7]*Research Center for Functional Materials, National Institute for Materials Science, Tsukuba 305-0044, Japan*
[8]*Department of Experimental Physics, Faculty of Fundamental Problems of Technology, Wrocław University of Science and Technology, Wyb.Wyspiańskiego 27, 50-370 Wrocław, Poland*

(Received 17 July 2024; revised 6 December 2024; accepted 14 January 2025; published 20 February 2025)

$MoTe_2$ monolayers and bilayers are unique within the family of van der Waals materials since they pave the way toward atomically thin infrared light-matter quantum interfaces, potentially reaching the important telecommunication windows. Here, we report emergent exciton polaritons based on $MoTe_2$ monolayers and bilayers in a low-temperature open microcavity in a joint experiment-theory study. Our experiments clearly evidence both the enhanced oscillator strength and enhanced luminescence of $MoTe_2$ bilayers, signified by a 38% increase of the Rabi splitting and a strongly enhanced relaxation of polaritons to low-energy states. The latter is distinct from polaritons in $MoTe_2$ monolayers, which feature a bottlenecklike relaxation inhibition. Both the polaritonic spin valley locking in monolayers and the spin-layer locking in bilayers are revealed via the Zeeman effect, which we map and control via the light-matter composition of our polaritonic resonances.

DOI: 10.1103/PhysRevLett.134.076902

Introduction—Two-dimensional semiconductors of transition metal dichalcogenides (TMDCs) are an excellent research platform for solid-state cavity quantum electrodynamics due to their strong light-matter interactions and intriguing spin-valley locking [1–3]. Their optical properties hinge on very robust valley excitons with binding energies of hundreds of meV [4–6]. Composite quasiparticles such as exciton polaritons in TMDC microcavity systems can inherit physical properties from both the cavity modes and the optically active material, including the ultralight effective mass [7], magnetic responses [8,9], and nonlinearities due to exchange correlation [10,11], dipolar interaction [12], phase space filling [13], and moiré confinement [14]. Therefore, they are remarkable systems to explore collective phenomena such as bosonic condensation [15,16], coherent light emission [17–20], polariton blockade [21,22], and correlated magnetism [23].

Among the TMDC family members, $MoTe_2$ features a unique band structure with both the monolayer (ML) and bilayer (BL) exhibiting a direct band gap [24–29]. The ground-state excitonic resonances lie in the near infrared spectral range ~1.1 μm [29,30], making $MoTe_2$ a good candidate for optoelectronic [31] and quantum optical applications [32] in the optical telecommunication window [33]. The extraordinary electronic properties [34,35] also render $MoTe_2$ a promising material for studies of integer and fractional (anomalous) (spin) quantum Hall effects [36–39]. However, the strong light-matter coupling regime of $MoTe_2$ has not received notable attention.

In this Letter, we demonstrate the first experimental measurements on the strong coupling of excitons in $MoTe_2$ ML and BL with discretized cavity modes in a low-temperature open optical microcavity. Our Letter reveals that the BL features an increase in Rabi splitting and coupling strength by 38% compared to the ML, while maintaining otherwise identical conditions. Interestingly, we observe a bottlenecklike inhibition of relaxation in ML structures, effectively enhancing the luminescence from the upper polariton branch (UPB), while, in stark contrast, the majority of the population relaxes to the lower polariton branch (LPB) in the BL. Our experiments are complemented by a many-particle theory revealing the

*Contact author: christian.schneider@uni-oldenburg.de

microscopic mechanisms behind this qualitatively different behaviour in $MoTe_2$ ML and BL. Using systematic magneto-optics measurements, we explore the polaritonic Zeeman effect and reveal g-factors controlled by the cavity-exciton detuning, manifesting the valley and layer degrees of freedom in the ML and BL, respectively. We also discover an unconventional enhancement of the coupling strength of both the ML and BL in the magnetic field.

Strong Coupling and Quasiparticle Relaxation—The $MoTe_2$ ML and BL are encapsulated [40] with thin hexagonal boron nitride flakes and deposited on a distributed Bragg reflector (DBR) with a stop band centered at 1050 nm, see Figs. S1(a), S1(b), and S1(e) of the Supplemental Material [41]. The samples are loaded in a closed-cycle low-temperature cryostat (3.5 K) equipped with a superconducting magnet. First, we perform the photoluminescence (PL) and differential reflectivity (DR) measurements on the encapsulated $MoTe_2$ flakes by using a linearly polarized 765 nm continuous wave laser and a tungsten-halogen lamp, respectively. The indiscernible Stokes shift between the PL and DR proves the high quality of our samples [see Figs. S1(f–i) [41]]. More experimental details are summarized in Section III of [41].

For strong coupling measurements, we use a top mirror that is a gold-coated silica mesa with a premanufactured spherical-cap shaped lens structure of 6 μm diameter and 300 nm depth [see Figs. S1(c) and S1(d) [41]]. A schematic of the cavity setting is shown in Fig. 1(a). The lens and bottom DBR form discretized Tamm-plasmon lens modes

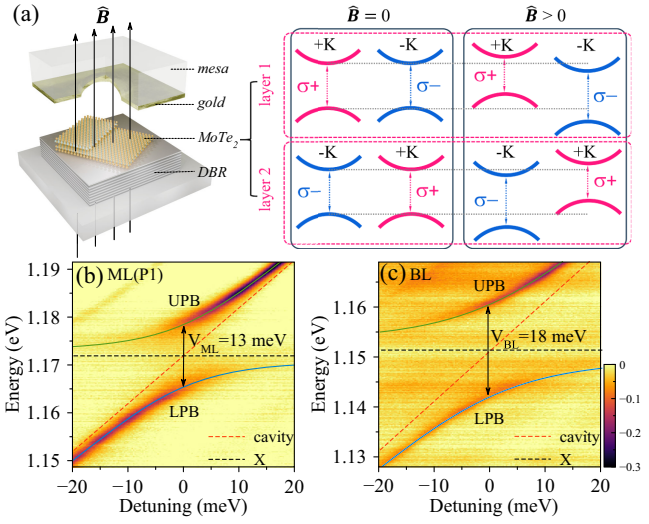

FIG. 1. (a) Schematic of the open cavity embedded with $MoTe_2$ ML and BL in a magnetic field. The valley Zeeman effect for layers with inversion symmetry is sketched in the right panel. (b) DR as a function of cavity detuning with a cavity loaded with a ML (P1), featuring exciton energy $E_X^{ML} = 1.1719$ eV and a Rabi splitting of $V_{ML}^{0T} = 13$ meV. (c) DR in BL as a function of cavity detuning, featuring $E_X^{BL} = 1.1513$ eV and $V_{BL}^{0T} = 18$ meV. Detuning is modified with a change of cavity length. The color bar is identical for (b) and (c).

(Q factors ~400) that can be readily measured in PL or DR. The focused excitation spots are comparable to the lens diameter. Our previous works have demonstrated the capability of discretized Tamm modes in tuning the emitters' spontaneous emission rates in the weak coupling regime [57,58]. A DC voltage applied to the actuator can change the cavity length with sub-nm positioning resolution. The PL and DR measurements are thus performed with a fine detuning step size of 0.1 meV. The detuning $\Delta = E_C - E_X$ is defined as the energetic difference between the cavity and exciton modes. Both measured ML and BL samples are deliberately tuned to couple with the eighth longitudinal lens mode, corresponding to a cavity length of approximately 4.28 μm at $\Delta = 0$.

In cavity-length dependent DR measurements in Figs. 1(b) and 1(c), we observe clear anticrossing features. We apply coupled oscillators theory to calculate the energy of both polariton branches as a function of the cavity-exciton detuning via $E_{UPB(LPB)} = (E_X + E_C \pm \sqrt{V^2 + \Delta^2})/2$, where V is the coupling strength. The fitting of polariton resonances in ML and BL are superimposed on the experimental DR results in Figs. 1(b) and 1(c), as well as in the PL measurements in Figs. 2(a) and 2(b). This approach yields a coupling strength of $V_{ML}^{0T} = 13$ meV for the $MoTe_2$ ML (position 1) and $V_{BL}^{0T} = 18$ meV for the BL. The superscript 0 T indicates the absence of an external magnetic field. We encounter a slight variation of the coupling strength for different sample positions of the ML on the order of the polariton linewidth (see Figs. S5 and S6 for measurements on different positions: P2 and P3 [41]). Indeed, the observed increase of the Rabi splitting by a factor of 1.38 for the BL is in agreement with the Tavis-Cummings model, which predicts a scaling with the square root of the number of oscillators [59–61].

A striking difference between ML and BL polaritons becomes apparent when comparing the PL intensity between the UPB and LPB in the two cases. Figure 2(a) depicts the PL from the polaritonic modes for the ML sample (P1), whereas the BL case is plotted in Fig. 2(b) with identical excitation conditions. For BL polaritons, the UPB emission is much weaker than the emission from the LPB, which is indicative of efficient relaxation of population to the energetically lower state. In stark contrast, for ML polaritons, the UPB is generally more intense than the LPB (see Fig. S5(a) and Fig. S6(a) for other sample positions [41]). We plot the emission intensity ratio between the UPB and LPB in Fig. 2(e) to quantify the relaxation strength for all detunings: in the BL case, the intensity ratio is generally smaller than 0.4, which is indicative of enhanced PL from the LPB, as a consequence of efficient relaxation. However, in the case of the ML, the ratio exceeds unity even for very red detuning and increases dramatically toward the zero and blue detuning regimes.

We model the polariton population and relaxation in our systems using a material-realistic many-particle

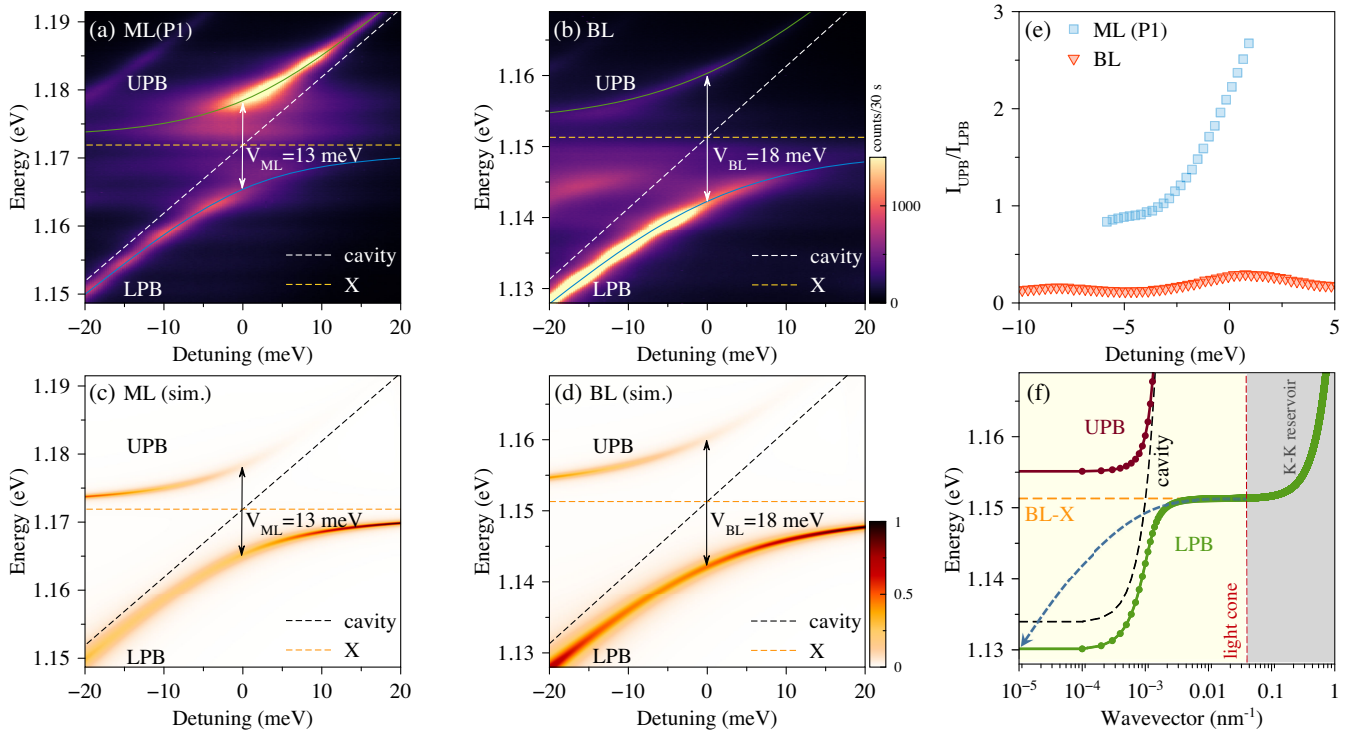

FIG. 2. PL spectra of exciton polaritons in (a) ML (P1) and (b) BL as a function of detuning. The ML polaritons feature a significant PL emission from the UPB, whereas BL polaritons exhibit substantial particle relaxation into the LPB. Note that the oscillatory intensity of the polariton branches is caused by detector etalon effects (see Fig. S3 of [41] for more details). Polariton energies extracted from the DR spectra using the coupled oscillator model are superimposed on the PL anticrossings, demonstrating excellent consistency. Theoretical description of the PL for (c) $MoTe_2$ ML and (d) BL polaritons, based on the material-realistic parameters from the experiments. Both absolute intensities are normalized to the BL emission, sharing the same color bar of (d). (e) Experimentally extracted PL intensity ratio between the UPB and LPB in $MoTe_2$ ML and BL as a function of the detuning. (f) Schematic of the polariton relaxation regime. The detuning is set to -17.5 meV to position the LPB ($k = 0$) 21 meV below the BL exciton, matching the energy of the homopolar A_1 optical phonons. The coupling strength and exciton energy at $k = 0$ are experimental values. The opening of relaxation to the LPB ($k = 0$) is marked by the blue dashed arrow.

theory [41]. Exciton polaritons are modeled within a Wannier-Hopfield framework [62], using the experimentally extracted light-matter coupling parameters and a bare cavity linewidth of 1.5 meV. Polariton-phonon scattering is described via the deformation potential and second-order Born-Markov approximation [63,64]. In particular, we explicitly account for the A_1 homopolar phonon with an energy of 21 meV, which strongly interacts with excitons in $MoTe_2$ [30,65]. The values for the deformation potentials are extracted from experimentally measured temperature-dependent linewidths of the 1s exciton in both ML and BL $MoTe_2$ (see Fig. S7 [41]). We find an increased exciton-phonon coupling for the BL, in agreement with previous studies [26]. The frequency-dependent PL at steady-state conditions is given by the polariton Elliot formula [63]

$$I(\omega) = \sum_{n=LPB,UPB} \frac{\gamma_n \Gamma_n}{(E_n - \hbar\omega)^2 + (\gamma_n + \Gamma_n)^2} N_n^0, \quad (1)$$

where γ and Γ are the polariton radiative and phonon-induced decay rates, respectively; E_n is the polariton energy; and N_n^0 is the Boltzmann distribution of the quasi particles. We fix the effective temperature of the exciton gas to 60 K to consider the realistic case of imperfect thermalization. The results of the model are plotted for the case of ML [Fig. 2(c)] and BL polaritons [Fig. 2(d)]. Strikingly, the dramatic increase of the lower polariton PL for the BL is well captured in our microscopic description, which verifies the impact of the A_1 phonon mode on the relaxation dynamics. The more efficient polariton relaxation observed for the BL is attributed to the combined effect of the enhanced exciton-phonon coupling and larger Rabi splitting. The BL polariton has a larger excitonic character at the negative detunings where the scattering channel from the exciton reservoir opens up [see Fig. 2(f)], i.e., $E_{\mathrm{LPB}} + E_{\mathrm{A_1}} \approx E_{\mathrm{X}}$, where E_{A_1} is the A_1 phonon energy. This, together with the larger exciton-phonon scattering in the BL, leads to a significantly larger occupation of the BL LPB at all detunings.

Polaritonic magneto optics—Polaritons are light-matter hybrid quasiparticles whose magnetic responses stem from their specific excitonic nature. The polaritonic g factor

thus needs to be rescaled by the excitonic Hopfield coefficient: $|X_k|^2 = (\sqrt{\Delta_k^2 + V^2} + \Delta_k)/2\sqrt{\Delta_k^2 + V^2}$, a parameter characterizing the excitonic proportion in the polariton. However, the polaritonic Zeeman phenomena in TMDCs have not been systematically studied with different light-matter compositions.

Due to time-reversal symmetry, the spin, orbital, and valley indices in the ML take opposite signs between adjacent K valleys, leading to a locking of spin and valley degrees of freedom in bands with strong spin-orbit coupling. In contrast, the BL retains the inversion symmetry, which leads to the intriguing phenomenon of spin-layer locking [66–68]. Both phenomena reveal distinctive spectral signatures in polarization spectroscopy in the presence of external magnetic fields, as sketched in Fig. 1(a). To extract the exciton out-of-plane g factor, magneto-DR measurements are performed between ±9 T in a Faraday geometry in the absence of the top mirror, ensuring weak coupling conditions. We utilize linearly polarized excitation, and measure counter-circularly polarized signals ($\sigma\pm$). The results are shown in Fig. S4 [41]. The out-of-plane excitonic g factors (g_x) are calculated by fitting the Zeeman splitting of the valley excitons by using $\Delta E = g_x \mu_B B$, where μ_B is the Bohr magneton and B is the magnetic flux density. The values of $g_X^{ML} = -4.6$ and $g_X^{BL} = -4.1$ are in excellent agreement with previous reports [69–71].

We notice that the modified sample position (P3) which is chosen for the magneto-optical study of the ML polaritons features a slightly larger coupling strength of 16 meV measured at zero field [see Fig. S3(a) and Figs. S5(a) and S5(b) [41]], which we attribute to locally varying dielectric screening and charging effects in the ML. Polaritonic Zeeman effects in both the $MoTe_2$ ML and BL are then extracted from magneto-PL measurements (Fig. 3). We utilize the same polarization configuration for the polaritonic magneto-optics measurements. The polaritonic Zeeman splitting as a function of the detuning is then straightforwardly calculated via the energetic differences between $\sigma+$ and $\sigma-$ resonances at +9 T.

We first plot the spectrally resolved detuning-dependent polarization patterns for ML and BL polaritons in Figs. 3(a) and 3(b), which are obtained by subtracting the $\sigma-$ polarized spectrum from the $\sigma+$ polarized spectrum at the same cavity detuning. The same effects are also revealed in the color-coded magneto-DR difference spectra that are compiled in Figs. S5(d) and S5(f) [41]. We can immediately see the detuning-dependent dichroism, which

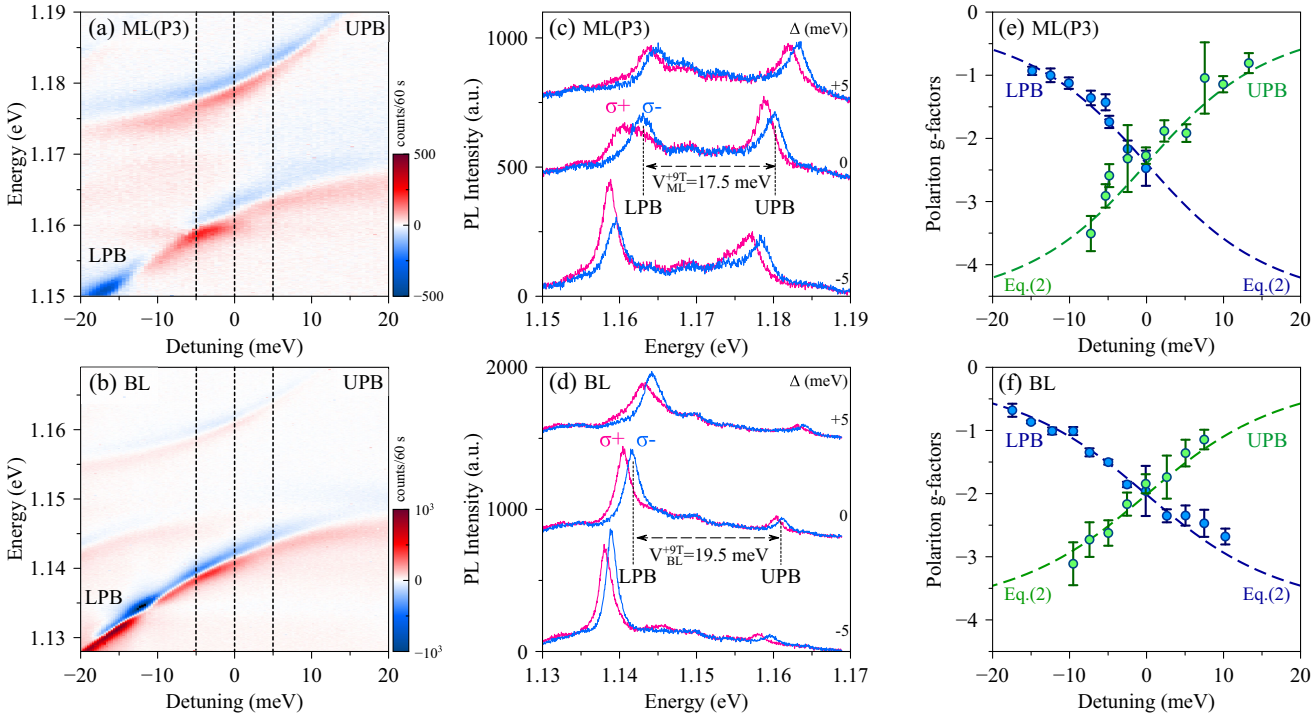

FIG. 3. Polariton Zeeman effect in spectrally and polarization-resolved PL measurements at +9 T. The color-coded Zeeman plots in (a) ML (P3) and (b) BL are obtained by subtracting the $\sigma-$ polarized spectrum from the $\sigma+$ polarized spectrum at the same cavity detuning. The high polarizaton of LPB around $\Delta = -10$ meV is due to trion states that couple to the exciton polaritons via the cavity resonance (see discussion in Section III of [41]). (c) ML (P3) and (d) BL representative PL spectra of polariton Zeeman splits at $\Delta = 0$ and ±5 meV, corresponding to the dashed lines in (a) and (b). The Rabi splittings are $V_{ML}^{+9T} = 17.5$ meV for the ML and $V_{BL}^{+9T} = 19.5$ meV for the BL. Experimental (dots) and theoretical (dashed lines) polariton g-factors in (e) ML (P3) and (f) BL. The error bars are derived by summing up the energetic error bars of the fitted polariton peaks in Figs. S5(c) and S5(e) [41].

becomes especially prominent in the excitonic regime of the polariton branches, for example, at $\Delta = \pm 20$ meV for the LPB and UPB, respectively. Magneto-PL and DR difference spectra from another sample position (P2) of the ML, which display the same polaritonic Zeeman effects, are presented in Fig. S6 [41].

The PL spectra at detunings of 0 and ± 5 meV are also shown in Fig. 3(c) for the ML case and Fig. 3(d) for the BL case. The Zeeman splitting becomes very apparent in this representation and acquires a similar magnitude for the ML and BL polaritons for comparable detunings. From the detuning-dependent Zeeman effect, we can model the UPB and LPB g factors as a function of detuning as

$$g_{UPB(LPB)} = \frac{g_x}{2} \pm \frac{\sqrt{V^2 + \Delta_1^2}}{2\mu_B B} \mp \frac{\sqrt{V^2 + \Delta_2^2}}{2\mu_B B}, \quad (2)$$

where $\Delta_1 = E_C - E_X^{\sigma^+}$ and $\Delta_2 = E_C - E_X^{\sigma^-}$ are the actual cavity detunings with respect to each excitonic Zeeman split, and $\Delta = (\Delta_1 + \Delta_2)/2$. The zero detunings of Δ_1 and Δ_2 are marked by double-sided arrows in Figs. S5(c) and S5(e) [41] that present the Lorentzian fitting results of the polariton Zeeman splits in ML and BL at +9 T. The experimentally extracted polaritonic g factors of each branch in the ML [Fig. 3(e)] and BL [Fig. 3(f)] are in excellent agreement with our theoretically derived values from Eq. (2). The degeneracy of the valley as well as the layer-locked polaritons in the ML and BL is thus lifted, while the strong coupling effect is verified as a viable tool to tune the resulting optical dichroism.

It is furthermore worth noting that, comparing the coupling strength at +9 T [Figs. 3(c) and 3(d)] to the scenario without the magnetic field (Figs. S3(b) and S3(h) [41]), the Rabi splittings are enhanced by 1.5 meV for both the ML and BL, corresponding to an effective enhancement of the coupling strength by approximately 8–9%. This behavior occurs consistently for various sample positions [see Figs. S6(e) and S6(f) [41]]. The coupling strength enhancement by magnetic field was previously reported for polaritons in III–V semiconductor quantum wells embedded in monolithic cavities [72], where the magnetic compression of exciton wave function increases the exciton oscillator strength and consequently enhances the vacuum-field Rabi splitting [73]. Our observation is thus very unconventional, since the exciton Bohr radius ($a_B \sim 1$–2 nm) is significantly smaller than the estimated magnetic length $L_B = \sqrt{\hbar/(e \cdot B)} \approx 8.6$ nm.

Conclusions—We report the first optical microscopy measurements on the emergence of exciton polaritons in $MoTe_2$ monolayer and bilayer. In contrast to the bilayer that exhibits an efficient population relaxation to the lower polariton branch, the relaxation in the monolayer features a pronounced bottleneck phenomenon, which has been modeled using a microscopic many-particle theory describing the scattering of exciton polaritons with A_1 optical phonons. We have also verified the strong couplings via magneto-optics measurements, where the polariton valley and layer degeneracies are lifted in the monolayer and bilayer, respectively. We can thus extract the polaritonic g factors as a function of the cavity-exciton detuning. Our Letter paves the way for further research involving cavity-mediated phenomena in $MoTe_2$-based van der Waals heterostructures, including the study of correlated phenomena, Telluride-based dipolaritons, and polariton lasers operated at telecommunication wavelengths.

Acknowledgments—The project is funded by Deutsche Forschungsgemeinschaft (DFG) Lantern project (funding numbers: Schn1376 11.1). C. S. acknowledges DFG within the initiative for major equipment (Project INST184-220). B. H. acknowledges Alexander von Humboldt-Stiftung for a fellowship grant. M. E. acknowledges funding from the Carl von Ossietzky Universität Oldenburg through a Carl von Ossietzky Young Researchers' Fellowship. F. E. acknowledges support by DFG SFB 1375 (NOA) and BMBF FKZs 16KISQ087K and 13XP5053A. J. F, R. R., and E. M. acknowledge funding from DFG via SFB 1083 and the regular project 524612380. K. W. and T. T. acknowledge support from the JSPS KAKENHI (Grant No. 21H05233 and 23H02052) and World Premier International Research Center Initiative (WPI), MEXT, Japan. M. S. acknowledges funding from Project No. 2019/35/B/ST5/04308 financed by the Polish National Science Center (NCN).

[1] G. Wang, A. Chernikov, M. M. Glazov, T. F. Heinz, X. Marie, T. Amand, and B. Urbaszek, Rev. Mod. Phys. **90**, 021001 (2018).
[2] C. Schneider, M. M. Glazov, T. Korn, S. Höfling, and B. Urbaszek, Nat. Commun. **9**, 2695 (2018).
[3] T. Mueller and E. Malic, npj 2D Mater. Appl. **2**, 29 (2018).
[4] K. F. Mak, C. Lee, J. Hone, J. Shan, and T. F. Heinz, Phys. Rev. Lett. **105**, 136805 (2010).
[5] A. Chernikov, T. C. Berkelbach, H. M. Hill, A. Rigosi, Y. Li, B. Aslan, D. R. Reichman, M. S. Hybertsen, and T. F. Heinz, Phys. Rev. Lett. **113**, 076802 (2014).
[6] R. Perea-Causin, D. Erkensten, J. M. Fitzgerald, J. J. Thompson, R. Rosati, S. Brem, and E. Malic, APL Mater. **10** (2022).
[7] I. Carusotto and C. Ciuti, Rev. Mod. Phys. **85**, 299 (2013).
[8] A. V. Larionov, V. D. Kulakovskii, S. Höfling, C. Schneider, L. Worschech, and A. Forchel, Phys. Rev. Lett. **105**, 256401 (2010).
[9] J. Fischer, S. Brodbeck, A. V. Chernenko, I. Lederer, A. Rahimi-Iman, M. Amthor, V. D. Kulakovskii, L. Worschech, M. Kamp, M. Durnev, C. Schneider, A. v. Kavokin, and S. Hofling, Phys. Rev. Lett. **112**, 093902 (2014).
[10] G. Lerario, A. Fieramosca, F. Barachati, D. Ballarini, K. S. Daskalakis, L. Dominici, M. De Giorgi, S. A. Maier, G. Gigli, S. Kéna-Cohen *et al.*, Nat. Phys. **13**, 837 (2017).

[11] A. Amo, J. Lefrère, S. Pigeon, C. Adrados, C. Ciuti, I. Carusotto, R. Houdré, E. Giacobino, and A. Bramati, Nat. Phys. **5**, 805 (2009).
[12] C. Louca, A. Genco, S. Chiavazzo, T. P. Lyons, S. Randerson, C. Trovatello, P. Claronino, R. Jayaprakash, X. Hu, J. Howarth *et al.*, Nat. Commun. **14**, 3818 (2023).
[13] K. W. Song, S. Chiavazzo, and O. Kyriienko, Phys. Rev. Res. **6**, 023033 (2024).
[14] L. Zhang, F. Wu, S. Hou, Z. Zhang, Y.-H. Chou, K. Watanabe, T. Taniguchi, S. R. Forrest, and H. Deng, Nature (London) **591**, 61 (2021).
[15] C. Anton-Solanas, M. Waldherr, M. Klaas, H. Suchomel, T. H. Harder, H. Cai, E. Sedov, S. Klembt, A. V. Kavokin, S. Tongay *et al.*, Nat. Mater. **20**, 1233 (2021).
[16] J. Kasprzak, M. Richard, S. Kundermann, A. Baas, P. Jeambrun, J. M. J. Keeling, F. Marchetti, M. Szymańska, R. André, J. Staehli *et al.*, Nature (London) **443**, 409 (2006).
[17] H. Shan, L. Lackner, B. Han, E. Sedov, C. Rupprecht, H. Knopf, F. Eilenberger, J. Beierlein, N. Kunte, M. Esmann *et al.*, Nat. Commun. **12**, 6406 (2021).
[18] E. Y. Paik, L. Zhang, G. W. Burg, R. Gogna, E. Tutuc, and H. Deng, Nature (London) **576**, 80 (2019).
[19] M. Wurdack, E. Estrecho, S. Todd, C. Schneider, A. G. Truscott, and E. A. Ostrovskaya, Phys. Rev. Lett. **129**, 147402 (2022).
[20] J. Zhao, R. Su, A. Fieramosca, W. Zhao, W. Du, X. Liu, C. Diederichs, D. Sanvitto, T. C. Liew, and Q. Xiong, Nano Lett. **21**, 3331 (2021).
[21] A. Delteil, T. Fink, A. Schade, S. Höfling, C. Schneider, and A. İmamoğlu, Nat. Mater. **18**, 219 (2019).
[22] G. Munoz-Matutano, A. Wood, M. Johnsson, X. Vidal, B. Q. Baragiola, A. Reinhard, A. Lemaître, J. Bloch, A. Amo, G. Nogues *et al.*, Nat. Mater. **18**, 213 (2019).
[23] J. Scherzer, L. Lackner, B. Han, B. Polovnikov, L. Husel, J. Göser, Z. Li, J.-C. Drawer, M. Esmann, C. Bennenhei, F. Eilenberger, K. Watanabe, T. Taniguchi, A. S. Baimuratov, C. Schneider, and A. Högele, arXiv:2405.12698.
[24] C. Ruppert, B. Aslan, and T. F. Heinz, Nano Lett. **14**, 6231 (2014).
[25] B. Aslan, I. M. Datye, M. J. Mleczko, K. Sze Cheung, S. Krylyuk, A. Bruma, I. Kalish, A. V. Davydov, E. Pop, and T. F. Heinz, Nano Lett. **18**, 2485 (2018).
[26] S. Helmrich, R. Schneider, A. W. Achtstein, A. Arora, B. Herzog, S. M. de Vasconcellos, M. Kolarczik, O. Schöps, R. Bratschitsch, U. Woggon *et al.*, 2D Mater. **5**, 045007 (2018).
[27] C. Robert, R. Picard, D. Lagarde, G. Wang, J. P. Echeverry, F. Cadiz, P. Renucci, A. Högele, T. Amand, X. Marie, I. C. Gerber, and B. Urbaszek, Phys. Rev. B **94**, 155425 (2016).
[28] I. G. Lezama, A. Arora, A. Ubaldini, C. Barreteau, E. Giannini, M. Potemski, and A. F. Morpurgo, Nano Lett. **15**, 2336 (2015).
[29] J. Kutrowska-Girzycka, E. Zieba-Ostój, D. Biegańska, M. Florian, A. Steinhoff, E. Rogowicz, P. Mrowiński, K. Watanabe, T. Taniguchi, C. Gies *et al.*, Appl. Phys. Rev. **9**, 041410 (2022).
[30] B. Han, C. Robert, E. Courtade, M. Manca, S. Shree, T. Amand, P. Renucci, T. Taniguchi, K. Watanabe, X. Marie *et al.*, Phys. Rev. X **8**, 031073 (2018).
[31] H. Zhao, M. T. Pettes, Y. Zheng, and H. Htoon, Nat. Commun. **12**, 6753 (2021).
[32] A. Kavokin, T. C. Liew, C. Schneider, P. G. Lagoudakis, S. Klembt, and S. Hoefling, Nat. Rev. Phys. **4**, 435 (2022).
[33] M. S. Ramzan and C. Cocchi, Nanomater. Nanotechnol. **13**, 2740 (2023).
[34] A. Jindal, A. Saha, Z. Li, T. Taniguchi, K. Watanabe, J. C. Hone, T. Birol, R. M. Fernandes, C. R. Dean, A. N. Pasupathy *et al.*, Nature (London) **613**, 48 (2023).
[35] Z. Pan, W. Xiong, J. Dai, Y. Wang, T. Jian, X. Cui, J. Deng, X. Lin, Z. Cheng, Y. Bai *et al.*, arXiv:2307.06001.
[36] F. Xu, Z. Sun, T. Jia, C. Liu, C. Xu, C. Li, Y. Gu, K. Watanabe, T. Taniguchi, B. Tong *et al.*, Phys. Rev. X **13**, 031037 (2023).
[37] J. Cai, E. Anderson, C. Wang, X. Zhang, X. Liu, W. Holtzmann, Y. Zhang, F. Fan, T. Taniguchi, K. Watanabe *et al.*, Nature (London) **622**, 63 (2023).
[38] H. Park, J. Cai, E. Anderson, Y. Zhang, J. Zhu, X. Liu, C. Wang, W. Holtzmann, C. Hu, Z. Liu *et al.*, Nature (London) **622**, 74 (2023).
[39] K. Kang, B. Shen, Y. Qiu, Y. Zeng, Z. Xia, K. Watanabe, T. Taniguchi, J. Shan, and K. F. Mak, Nature (London) **628**, 522 (2024).
[40] A. Castellanos-Gomez, M. Buscema, R. Molenaar, V. Singh, L. Janssen, H. S. Van Der Zant, and G. A. Steele, 2D Mater. **1**, 011002 (2014).
[41] See Supplemental Material at http://link.aps.org/supplemental/10.1103/PhysRevLett.134.076902, which includes Refs. [42–51] for the microscopic theory and fitting of the experimental linewidths, Refs. [52–54] for further details on the strong coupling with higer order cavity modes, and Refs. [55,56] for the dicussion of the high polarization at detunings around −10 meV.
[42] G. Berghäuser and E. Malic, Phys. Rev. B **89**, 125309 (2014).
[43] S. Brem, J. Zipfel, M. Selig, A. Raja, L. Waldecker, J. D. Ziegler, T. Taniguchi, K. Watanabe, A. Chernikov, and E. Malic, Nanoscale **11**, 12381 (2019).
[44] A. Laturia, M. L. Van de Put, and W. G. Vandenberghe, npj 2D Mater. Appl. **2**, 6 (2018).
[45] S. Helmrich, K. Sampson, D. Huang, M. Selig, K. Hao, K. Tran, A. Achstein, C. Young, A. Knorr, E. Malic *et al.*, Phys. Rev. Lett. **127**, 157403 (2021).
[46] A. Raja, M. Selig, G. Berghauser, J. Yu, H. M. Hill, A. F. Rigosi, L. E. Brus, A. Knorr, T. F. Heinz, E. Malic *et al.*, Nano Lett. **18**, 6135 (2018).
[47] A. Kormányos, G. Burkard, M. Gmitra, J. Fabian, V. Zólyomi, N. D. Drummond, and V. Fal'ko, 2D Mater. **2**, 022001 (2015).
[48] T. Goldstein, S.-Y. Chen, J. Tong, D. Xiao, A. Ramasubramaniam, and J. Yan, Sci. Rep. **6**, 28024 (2016).
[49] B. Ferreira, R. Rosati, J. M. Fitzgerald, and E. Malic, 2D Mater. **10**, 015012 (2022).
[50] M. Selig, G. Berghäuser, A. Raja, P. Nagler, C. Schüller, T. F. Heinz, T. Korn, A. Chernikov, E. Malic, and A. Knorr, Nat. Commun. **7**, 13279 (2016).
[51] M. Selig, G. Berghäuser, M. Richter, R. Bratschitsch, A. Knorr, and E. Malic, 2D Mater. **5**, 035017 (2018).
[52] J. Wang, H. Xu, R. Su, Y. Peng, J. Wu, T. C. Liew, and Q. Xiong, Light Sci. Appl. **10**, 45 (2021).
[53] M. Dusel, S. Betzold, O. A. Egorov, S. Klembt, J. Ohmer, U. Fischer, S. Höfling, and C. Schneider, Nat. Commun. **11**, 2863 (2020).

[54] D. Horneber, J. Düreth, T. Schembri, S. Betzold, M. Stolte, S. Höfling, F. Würthner, and S. Klembt, arXiv:2409.12093.
[55] C. Rupprecht, E. Sedov, M. Klaas, H. Knopf, M. Blei, N. Lundt, S. Tongay, T. Taniguchi, K. Watanabe, U. Schulz *et al.*, 2D Mater. **7**, 035025 (2020).
[56] P. Back, M. Sidler, O. Cotlet, A. Srivastava, N. Takemura, M. Kroner, and A. Imamoğlu, Phys. Rev. Lett. **118**, 237404 (2017).
[57] J.-C. Drawer, V. N. Mitryakhin, H. Shan, S. Stephan, M. Gittinger, L. Lackner, B. Han, G. Leibeling, F. Eilenberger, R. Banerjee *et al.*, Nano Lett. **23**, 8683 (2023).
[58] B. Han, C. C. Palekar, F. Lohof, S. Stephan, V. N. Mitryakhin, J.-C. Drawer, A. Steinhoff, L. Lackner, M. Silies, B. Rosa *et al.*, Photonics Res. **13**, 210 (2024).
[59] C. Rupprecht, M. Klaas, H. Knopf, T. Taniguchi, K. Watanabe, Y. Qin, S. Tongay, S. Schröder, F. Eilenberger, S. Höfling *et al.*, Opt. Express **28**, 18649 (2020).
[60] M. Król, K. Rechcińska, K. Nogajewski, M. Grzeszczyk, K. Łempicka, R. Mirek, S. Piotrowska, K. Watanabe, T. Taniguchi, M. R. Molas *et al.*, 2D Mater. **7**, 015006 (2019).
[61] M. Tavis and F. W. Cummings, Phys. Rev. **170**, 379 (1968).
[62] J. M. Fitzgerald, J. J. Thompson, and E. Malic, Nano Lett. **22**, 4468 (2022).
[63] J. M. Fitzgerald, R. Rosati, B. Ferreira, H. Shan, C. Schneider, and E. Malic, Optica **11**, 1346 (2024).
[64] S. Brem, A. Ekman, D. Christiansen, F. Katsch, M. Selig, C. Robert, X. Marie, B. Urbaszek, A. Knorr, and E. Malic, Nano Lett. **20**, 2849 (2020).
[65] C. J. Sayers, A. Genco, C. Trovatello, S. D. Conte, V. O. Khaustov, J. Cervantes-Villanueva, D. Sangalli, A. Molina-Sanchez, C. Coletti, C. Gadermaier *et al.*, Nano Lett. **23**, 9235 (2023).
[66] A. M. Jones, H. Yu, J. S. Ross, P. Klement, N. J. Ghimire, J. Yan, D. G. Mandrus, W. Yao, and X. Xu, Nat. Phys. **10**, 130 (2014).
[67] S. Raiber, P. E. Faria Junior, D. Falter, S. Feldl, P. Marzena, K. Watanabe, T. Taniguchi, J. Fabian, and C. Schüller, Nat. Commun. **13**, 4997 (2022).
[68] M. Brotons-Gisbert, H. Baek, A. Molina-Sánchez, A. Campbell, E. Scerri, D. White, K. Watanabe, T. Taniguchi, C. Bonato, and B. D. Gerardot, Nat. Mater. **19**, 630 (2020).
[69] C. Jiang, F. Liu, J. Cuadra, Z. Huang, K. Li, A. Rasmita, A. Srivastava, Z. Liu, and W.-B. Gao, Nat. Commun. **8**, 802 (2017).
[70] A. Arora, M. Drüppel, R. Schmidt, T. Deilmann, R. Schneider, M. R. Molas, P. Marauhn, S. Michaelis de Vasconcellos, M. Potemski, M. Rohlfing *et al.*, Nat. Commun. **8**, 639 (2017).
[71] M. Goryca, J. Li, A. V. Stier, T. Taniguchi, K. Watanabe, E. Courtade, S. Shree, C. Robert, B. Urbaszek, X. Marie *et al.*, Nat. Commun. **10**, 4172 (2019).
[72] J. D. Berger, O. Lyngnes, H. M. Gibbs, G. Khitrova, T. R. Nelson, E. K. Lindmark, A. V. Kavokin, M. A. Kaliteevski, and V. V. Zapasskii, Phys. Rev. B **54**, 1975 (1996).
[73] A. V. Kavokin, J. J. Baumberg, G. Malpuech, and F. P. Laussy, *Microcavities* (Oxford University Press, New York, 2017), Vol. 21.